Smart Mattress Based on Multipoint Fiber Bragg Gratings for Respiratory Rate Monitoring

Francesca De Tommasi, *Student Member, IEEE*, Daniela Lo Presti, *Member, IEEE*, Michele Arturo Caponero, Massimiliano Carassiti, Emiliano Schena, *Senior Member, IEEE*, and Carlo Massaroni, *Senior Member, IEEE*

***Abstract*— Long-term monitoring of respiratory rate (RR) is of great importance in people suffering from sleep-related breathing disorders (SBDs). Instrumented mattresses are gaining the attention of several research groups to monitor this vital sign. Among the existing sensing techniques, fiber Bragg grating sensors (FBGs) show promise in this arena. In this article, we presented a novel FBG-based smart mattress to monitor RR over time. The proposed measuring system consisted of 13 sensing elements (SEs) based on FBGs encapsulated in soft biocompatible rubber, totally embedded in multiple silicone layers. Compactness, robustness, and user comfort are the main advantages of our solution. The mattress size and the arrangement of the 13 SEs were chosen to allow monitoring subjects with different anthropometric parameters and taking up different sleeping postures. Before the overall system integration, each SE was subjected to static and dynamic metrological characterization, a process often overlooked in fiber-optic-based mattresses. Results showed a mean sensitivity to force equal to 14 pm · N^{-1} and a mean percentage hysteresis error always lower than 18%. The feasibility assessment of the system in RR monitoring was carried out on five healthy volunteers taking up common sleeping postures (i.e., supine -S-, right side -RS-, left side -LS-, and prone -P-) under two breathing conditions (i.e., quiet breathing -QB-, and tachypnea -T-). RR estimation showed a mean absolute error (MAE) always lower than 0.65 breaths/min. The promising findings proved the capability of our smart mattress in monitoring RR over time, encouraging the investigation of its performance in real-world scenarios.**

***Index Terms*— Fiber Bragg grating sensors (FBGs), multipoint monitoring, respiratory rate (RR), smart mattress, unobtrusive monitoring.**

I. Introduction

SLEEP-RELATED breathing disorders (SBDs) are a growing health problem worldwide and the most prevalent of all existing sleep illnesses, especially in the elderly population [1], [2]. People suffering from these pathologies complain of troublesome sleep, often characterized by snoring and prolonged obstructive apnea, resulting in a poor quality of life and, in worst cases, even in depression [3], [4]. Numerous scientific studies have also demonstrated a high incidence of cardiovascular diseases (e.g., stroke and ischemia) associated with SBDs, underscoring the severity of this issue [5], [6]. Obstructive sleep apnea syndrome (OSAS) is characterized by recurrent blockage of the upper airway leading to oxygen desaturation and awakenings in sleep [7]. Therefore, long-term monitoring of respiratory waveform and respiratory rate (hereafter RR) can be of paramount importance in the prevention and diagnosis of such diseases [8], [9].

Currently, polysomnography represents the gold standard for the investigation and evaluation of SBDs, requiring overnight patient hospitalization. It demands the placement of several sensors and electrodes on the patient's body to monitor different physiological parameters including respiratory pattern and RR [10], [11]. Nevertheless, this bulky instrumentation results in total discomfort for the patients and the potential for unreliable measurements [12]. In the last years, unobtrusive technologies are fostering increasing interest in this scenario [1]. COVID-19 pandemic has boosted the trend of unobtrusive and remote monitoring of patients' health status due to the limited access to hospital facilities [13]. The possibility of monitoring patients in an unstructured environment, without the presence of highly specialized equipment, and avoiding the placement of cumbersome instrumentation on the patient's body makes unobtrusive techniques very attractive [14]. Both contact-based and contactless technologies have been espoused in this field [15], [16], [17], [18]. Over the past decades, among the existing unobtrusive technologies, the development of instrumented mattresses for respiratory monitoring gathered the attention of several research groups and companies [19], [20], [21], [22], [23], [24], [25], [26], [27], [28], [29], [30], [31], [32], [33], [34], [35], [36], [37], [38], [39], [40], [41], [42], [43], [44], [45], [46]. In this framework, a wide range of sensing solutions have been explored including strain [21], [23], [34], [41], [42], [44], pressure [20], [22], [24], [25], [26], [28], [33], [35], force [27], [36], capacitive sensors [37], and different types of fiber-optic-based systems [e.g., plastic optical fibers, Mach–Zender interferometers, microbend fiber-optic sensors, and fiber Bragg grating sensors (FBGs)] [29], [30], [31], [32], [38], [39], [40], [43], [45], [46]. Unfortunately, these solutions encounter some disadvantages involving several aspects, especially missing

Manuscript received 21 July 2022; revised 20 October 2022; accepted 10 December 2022. Date of publication 27 December 2022; date of current version 12 January 2023. The Associate Editor coordinating the review process was Dr. Yuya Koyama. *(Corresponding author: Carlo Massaroni.)*

This work involved human subjects or animals in its research. Approval of all ethical and experimental procedures and protocols was granted by Ethical Committee of our Institution under Application No. ST-UCBM 27/18 OSS, and performed in line with the Declaration of Helsinki.

Francesca De Tommasi, Daniela Lo Presti, Emiliano Schena, and Carlo Massaroni are with the Unit of Measurements and Biomedical Instrumentation, Departmental Faculty of Engineering, Università Campus Bio-Medico di Roma, 00128 Rome, Italy (e-mail: c.massaroni@unicampus.it).

Michele Arturo Caponero is with the ENEA Research Center of Frascati, 00044 Rome, Italy.

Massimiliano Carassiti is with the Unit of Anesthesia, Intensive Care and Pain Management, School of Medicine, Università Campus Bio-Medico di Roma, 00128 Rome, Italy.

This article has supplementary downloadable material available at https://doi.org/10.1109/TIM.2022.3232615, provided by the authors.

Digital Object Identifier 10.1109/TIM.2022.3232615

consideration of anthropometric variability among subjects in the selection of mattress size, poor sensors integrability in the measurement system, and disregard of metrological aspects at the manufacturing stage.

Out of all proposed technologies, fiber optic sensors benefit from some inherent advantages over electrical sensors for the development of instrumented mattresses.

Among others, biocompatibility, reduced size, high flexibility, inherent safety, long-term stability, humidity resistance, high sensitivity, fast response time, and, above all, immunity to electromagnetic fields. This latter feature makes optical sensors suitable in clinical scenarios since they can operate in harsh environments [e.g., magnetic resonance imaging (MRI)] without interference. On the other hand, electrical sensors typically lack all such qualities because of their low safety, high electromagnetic disturbance capacity, poor stability, easy deterioration and corrosion, and less performance, which hardly qualifies them for long-term applications. Among different types of optical sensors, FBGs are gaining momentum in a plethora of medical applications [47], [48]. Their rapid spread is warranted not only by the countless peculiarities of fiber optics, but also by their multiplexing capability allowing them to accommodate a multitude of sensors within a single fiber. Moreover, the FBG's encapsulation into silicone rubbers may increase their robustness and flexibility. In the literature, instrumented mattresses based on FBG sensors account for a small fraction of the several proposed [29], [30], [31], [46]. The presented solutions include respiratory monitoring during MRI by means of a single FBG on a plexiglass board [30], [31] and the deployment of arc-shaped pressure sensors placed directly on the bed surface [29]. A first attempt at the development of FBG-based mattresses was carried out also by our research group to investigate the feasibility of this solution for RR monitoring [46].

Here, we reported a novel smart mattress based on multiple distributed sensing elements (SEs) consisting of FBGs encapsulated in silicone rubber to measure RR over time. The original solution presents a sandwich structure made of different layers of silicone and nitrile butadiene rubbers (NBRs), ensuring robustness, compactness, and high comfortability of the device. Unlike other FBG-based solutions, our design was conceived considering the anatomical variability among subjects, allowing the instrumentation of the body portions most affected by deformations caused by breathing. Moreover, we assessed the response of each SE to force (F) in both static and dynamic conditions, a praxis often lacking in these kinds of solutions. Finally, we investigated the feasibility of the smart mattress for RR monitoring on five healthy volunteers and the influence of common sleeping postures (i.e., supine -S-, right side -RS-, left side -LS-, and prone -P-) and breathing stages (i.e., quiet breathing -QB-, and tachypnea -T-) on the performance of the proposed measuring system.

This article is structured as follows. Section II describes the FBG's working principle, the design and fabrication of the SEs, and the metrological characterization process to assess the F sensitivity values of each SE and their hysteresis error. Section III reports the design and development of the smart mattress embedding the 13 SEs and the feasibility evaluation on healthy volunteers. Finally, Sections IV and V discuss the results obtained and conclude by outlining the main remarks of our study, limitations, and future perspectives.

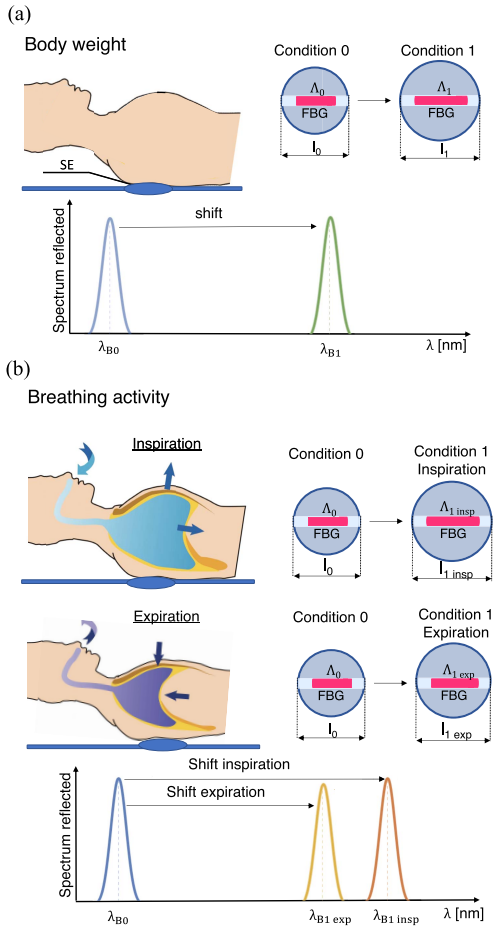

Fig. 1. As an example, spectrum and Λ changes of one SE caused by (a) presence of the body and (b) inspiration and expiration phases of the breathing activity.

II. FBG-Based SEs: Design, Fabrication, and Metrological Characterization

An FBG sensor works as a stopband filter imprinted inside an optical fiber. During its manufacturing, a portion of the optical fiber core is exposed to a variable pattern of intense UV laser light, thus inducing a permanent periodic perturbation of the effective refractive index (n_{eff}) [49]. When a light signal scans the optical fiber via an optical interrogator, the periodic variation of n_{eff} leads to a reflection of narrow wavelengths portion centered around the FBG operating wavelength (i.e., Bragg wavelength, λ_B), fulfilling the following relationship [50]:

$$\lambda_B = 2 \cdot n_{\text{eff}} \cdot \Lambda \tag{1}$$

where Λ denotes the spatial grating period.

The working principle of FBG lies in a shift of λ_B (hereafter $\Delta\lambda_B$) caused by a mutation in Λ and n_{eff}. So, $\Delta\lambda_B$ can occur when the fiber is exposed to strain (ϵ) or temperature

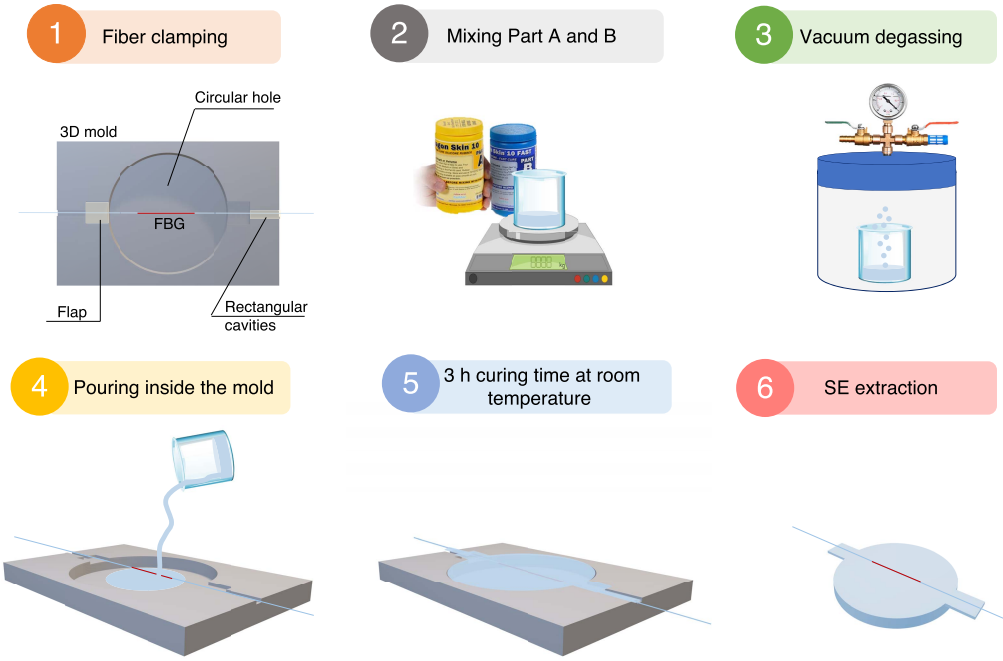

Fig. 2. Manufacturing steps of one of the 13 SEs consisting of (1) fiber clamping and pulling; (2) mixing Parts A and B; (3) vacuum degassing; (4) pouring inside the mold; (5) 3 h curing time at room temperature; and (6) SE extraction.

variations (ΔT), according to the following equation [51]:

$$\Delta\lambda_B = 2\left[\Lambda\frac{\partial n_{\text{eff}}}{\partial\epsilon} + n_{\text{eff}}\frac{\partial\Lambda}{\partial\epsilon}\right]\Delta\epsilon + 2\left[\Lambda\frac{\partial n_{\text{eff}}}{\partial T} + n_{\text{eff}}\frac{\partial\Lambda}{\partial T}\right]\Delta T \tag{2}$$

where the first addendum relates to the effect of strain and the second one to the influence of temperature on the optical fiber. Focusing on the framework of our study, temperature changes due to the physical presence of body parts on the mattress are considered negligible compared to chest wall deformations during breathing. Such consideration can be assumed keeping in mind the different dynamics of the two signals (i.e., breathing and temperature variations). Actually, breathing content may be assumed to be a periodic signal, whereas body temperature variations can be considered a quasi-static signal. Moreover, it is worth noting that each SE was enclosed within a higher layer of silicone rubber and subsequently covered with nitrile rubber (as detailed in Section III-A) and, thus, out of direct contact with the human body. The SE output is influenced by both the body weight of the user lying on the surface and the breathing activity (see Fig. 1). The presence of the body causes a precompression of the SE and in turn a shift in the reflected spectrum (Condition 1) with respect to the initial state (Condition 0) [Fig. 1(a)]. In addition, the expiratory and inspiratory phases of breathing act on the SE causing changes in its output. In particular, during inspiration, the chest expands because of air inhaling, resulting in a squeezing of the SE with a consequent strain increasing Λ [from Λ_0 to $\Lambda_{1\text{insp}}$; see Fig. 1(b)] and a shift (i.e., $\Delta\lambda_B$) in the reflected spectrum from λ_{B0} to $\lambda_{B1\text{insp}}$ ($\lambda_{B1\text{insp}} > \lambda_{B0}$). Then, during the expiratory phase, the chest shrinks due to the air exhalation: in this phase, the SE releases resulting in a decrease of the $\Lambda_{1\text{exp}}$ and consequent λ_B shift from $\lambda_{B1\text{insp}}$ to $\lambda_{B1\text{exp}}$ ($\lambda_{B0} < \lambda_{B1\text{exp}} < \lambda_{B1\text{insp}}$) in the reflected spectrum [see Fig. 1(b)].

A. Design and Fabrication

An array of multipoint FBGs was used for the development of the proposed smart mattress. The commercial array consisted of 13 polyimide-coated FBGs, each 10 mm long and spaced 4 cm apart with λ_B ranging from 1512 to 1568 nm and reflectivity values within 91% and 94% (AtGrating Technologies, Shenzhen, China). Before the whole mattress manufacturing, 13 SEs were produced. Ad hoc 3D molds were designed in a CAD environment (OnShape, PTC Inc., Boston, MA, USA) and then printed in polylactic acid (PLA) using a 3D printer (Ultimaker S2+). The mold consisted of a circular hole (with a diameter of 22 mm and a thickness of 2 mm) fashioned to fit the desired shape, two rectangular cavities to facilitate the clamping of the optical fiber inside the mold, and two flaps for facilitating the removal of the SE when ready [as detailed in Fig. 2(1)]. The optical fiber was clamped within the rectangular cavities of each mold ensuring the position of the FBG in the middle of the circular hole. The fiber was then pulled to avoid undesirable bending during the pouring phase of the silicone rubber. Once the FBGs were properly placed [Fig. 2(1)], Parts A and B of a DragonSkin10 were mixed in the same weight quantity [Fig. 2(2)] as suggested by the manufacturer, degassed to eject the air bubbles inside [Fig. 2(3)], and poured inside the mold [Fig. 2(4)]. A 3-h curing time was required for rubber polymerization [Fig. 2(5)] after which the polymeric matrix was safely released from the mold [Fig. 2(6)]. This procedure was carried out 13 times to obtain the 13 SEs. At the end of the fabrication, the fiber with the 13 SEs was extracted. Since the FBGs are intrinsically strain sensors, this stage of fabrication allowed us to employ SEs as force ones.

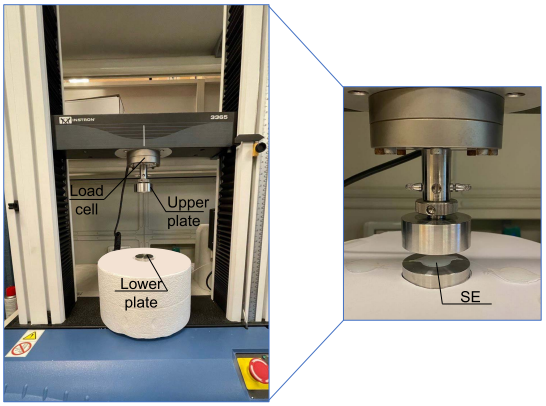

Fig. 3. Testing machine and positioning of the SE on its lower plate.

B. Metrological Characterization

Each SE underwent a metrological characterization process separately, both static and dynamic. Compression tests were performed by means of a testing machine (model 3365, Instron,[1] Norwood, MA, USA) equipped with a load cell (full-scale value 500 N and accuracy of ±0.25% of the reading value).

Static tests were carried out to evaluate the response of each SE to an external F and calculate its sensitivity. After placing the SE on the lower plate of the machine (as evidenced in Fig. 3), F in the range 0–20 N was applied with the upper plate at a displacement rate of 1 mm · min^{-1} to simulate quasi-static condition. Six compression tests were repeated to further investigate the mean sensitivity and relative uncertainty. During the tests, F values were recorded at a sampling rate of 100 Hz, and simultaneously SE response in terms of $\Delta\lambda_B$ was acquired at the same sampling rate through an optical interrogator (si255, Hyperion Platform, Micro Optics Inc., Atlanta, GA, USA). Later on, data were postprocessed in a MATLAB environment to obtain the calibration curve ($\Delta\lambda_B$ vs. F). $\Delta\lambda_B$ trends as a function of F were obtained for each compression test. The averaged values of $\Delta\lambda_B$ and the related uncertainty across the six compression tests were obtained. The uncertainty was estimated considering the T-student distribution with five degrees of freedom and a confidence level of 95%. The sensitivity to F of each SE (i.e., S_F) was estimated by fitting data with a linear model and the interpolation goodness was evaluated in terms of correlation coefficient (i.e., R^2), reported in Table I. The results obtained show S_F values ranging between 10 pm · N^{-1} and 18 pm · N^{-1} with R^2 equal or even greater than 0.99. The calibration curves for all SEs (from SE1 to SE13) are reported in Supplementary Materials.

Dynamic tests were performed to calculate the hysteresis errors. Each SE underwent nine cyclic compression tests (each consisting of a loading phase 0–20 N and an unloading phase 20–0 N) at four frequencies mimicking four different RRs (i.e., 12, 24, 36, and 60 breaths/min). These frequency values were chosen to simulate normal breathing stages (QB and T) [52] as well as RR outside the normal physiological range (i.e., 60 breaths/min). Both F and $\Delta\lambda_B$ data were acquired at a sampling rate of 100 Hz. After the data collection, the central seven cycles were considered to calculate the hysteresis error (Hyst$_{\text{err}}$%) as the ratio between the maximum distance value in terms of $\Delta\lambda_B$ between the loading and unloading phases at the same force input ($\Delta\lambda_B^{\text{loading}} - \Delta\lambda_B^{\text{unloading}}$) and the maximum $\Delta\lambda_B$ of the loading phase max($\Delta\lambda_B^{\text{loading}}$) for the given compression cycle, according to the following:

$$\text{Hyst}_{\text{err}}\% = \frac{\Delta\lambda_B^{\text{loading}} - \Delta\lambda_B^{\text{unloading}}}{\max\left(\Delta\lambda_B^{\text{loading}}\right)} \cdot 100. \tag{3}$$

The mean percentage hysteresis error ($\overline{\text{Hyst}_{\text{err}}\%}$) for all RRs was calculated as the average of the Hyst$_{\text{err}}$% values across the seven cycles. The relative uncertainty was estimated as previously for the static calibration curves (T-student distribution, six degrees of freedom, and confidence level of 95%). In Fig. 4, we report the mean percentage hysteresis error for each SE (distinguished by different colors, from blue to red) at 12 breaths/min [Fig. 4(a)], 24 breaths/min [Fig. 4(b)], 36 breaths/min [Fig. 4(c)], and 60 breaths/min [Fig. 4(d)]. Results showed $\overline{\text{Hyst}_{\text{err}}\%}$ always lower than

[1]Registered trademark.

TABLE I
FORCE SENSITIVITY VALUES AND CORRELATION COEFFICIENTS

SE	S_F [pm· N^{-1}]	R^2
1	15	0.997
2	12	0.991
3	11	0.996
4	14	0.993
5	12	0.993
6	16	0.995
7	18	0.994
8	17	0.990
9	14	0.985
10	10	0.997
11	13	0.993
12	13	0.998
13	12	0.988

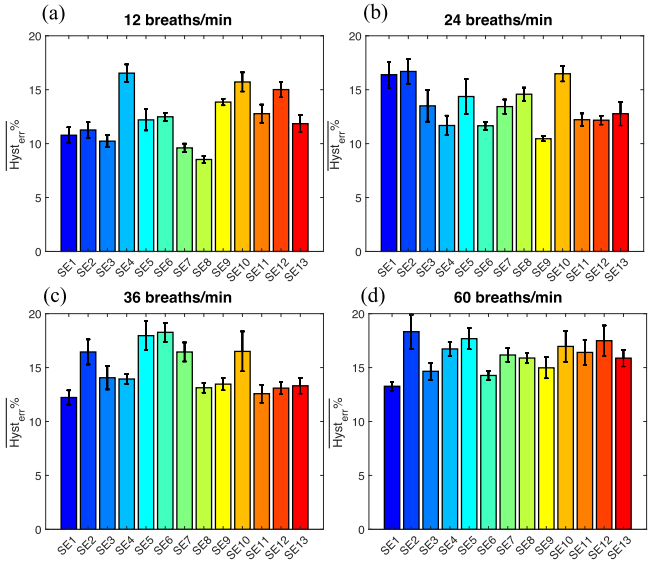

Fig. 4. $\overline{\text{Hyst}_{\text{err}}\%}$ and its uncertainty obtained per each SE at all the simulated RRs (i.e., (a) 12, (b) 24, (c) 36, and (d) 60 breaths/min).

approximately 18% and similar values at the different simulated RR.

III. Smart Mattress: Design, Development, and Validation

After the metrological characterization of the SEs, we first developed the multilayers smart mattress and then feasibility assessed it in-lab on healthy volunteers.

A. Design and Development

The proposed smart mattress was geometrically designed to be suitable for use on subjects of different stature and anthropometry and to fit the beds commonly used for clinical and home care use. According to [53], the longer side dimension was chosen considering the literature-available body anthropometric proportions between upper-mid trunk height (h_t) and the total height (h) [53]

$$h_t = 0.818 \cdot h - 0.530 \cdot h = 0.288 \cdot h \tag{4}$$

where $0.818 \cdot h$ refers to shoulder-foot height, and $0.530 \cdot h$ the lower trunk, upper, and lower leg height. By assuming that the upper and mid compartment of the trunk are the most affected by deformations caused by breathing activity [54], we decided to develop a rectangular-shaped mattress with dimensions of 500 × 400 mm ensuring that almost the entire h_t is resting on the mattress (even in the case of 190 cm tall subjects and different body posture assumed during sleeping). To develop the smart mattress, several manufacturing processes have been carried out to realize the sandwich structure and assemble the four layers of different materials. The first layer of the proposed mattress consisted of a 1 mm-thick silicone rubber DragonSkin30. This layer served as a support surface for the fiber and SEs integration. Before silicone pouring, 13 3D-printed circular molds (22 mm in diameter and 1 mm in width) were arranged on rigid plywood support at the intended locations for SEs placement to leave a cavity for their housing [Fig. 5(a)]. These molds were arranged to reproduce a serpentine pattern that allows SE distribution over a large area, thus fostering RR monitoring even in the case of different postures and subjects with different anatomical characteristics. Likewise for SEs, the two DragonSkin30 components were mixed in the same proportions, degassed, poured, and cured at room temperature for 16 h, as suggested in [55]. After the curing phase, the layer was peeled off and flipped back from the side where the cavities appeared after the circular molds removing [see Fig. 5(b)]. Before moving on to the next steps, the noninstrumented extremities of the optical fiber array were reinforced with a 900-μm Teflon jacket and connected to MU/APC adapters allowing the link of both ends to the optical interrogator. At this stage, the fiber with the SEs was laid out in a serpentine pattern. Each SE was plunked into the previously created holes by dropping SE1 (i.e., the one with the lowest λ_B) into the bottom of the rectangular layer and arranging the rest accordingly [see Fig. 5(c)]. Then, a second 2 mm-thick layer of DragonSkin10 rubber was added to ensure the successful embedding of all SEs inside [Fig. 5(d)]. The manufacturing process was performed for

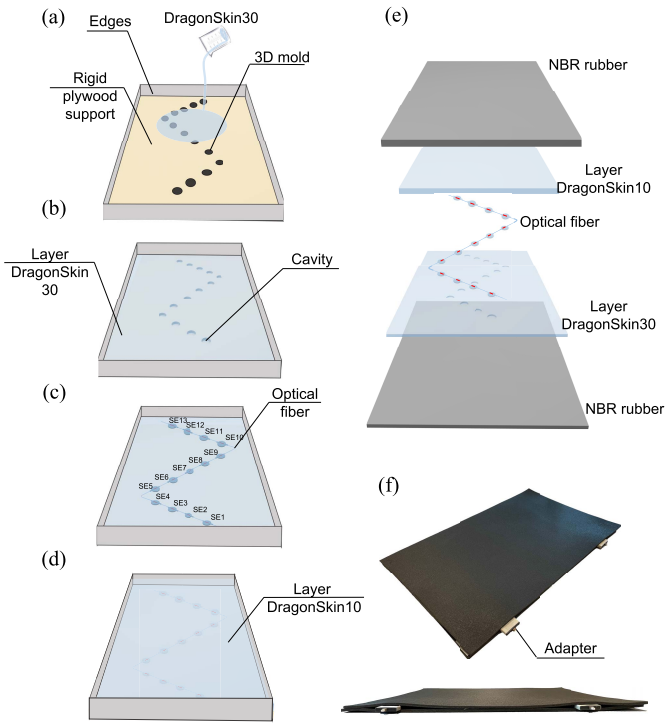

Fig. 5. Smart mattress manufacturing process. (a) Placement of rigid plywood support with edges and 13 molds for fabrication of the first layer of DragonSkin30. (b) Layer flipping on the cavity side. (c) Arrangement of 13 SEs in a serpentine pattern. (d) Pouring of DragonSkin10 for top layer fabrication. (e) Different layers of the smart mattress. (f) Photograph of the smart mattress ready to be validated.

the first layer. DragonSkin10 was used to form the mat's top layer (i.e., the one closest to the human body), while DragonSkin30 was for the bottom one (i.e., the one furthest from the body). DragonSkin10 allows better transmission of breathing-related deformations to the SEs, being more flexible than DragonSkin30, and prevents their mechanical dampening on the bottom surface. Later on, two layers of NBR measuring 500 × 800 mm were added to the previous layers and bonded together using double-sided adhesive tape [see Fig. 5(e)]. The final smart mattress ready to be validated is shown in Fig. 5(f).

B. Feasibility Assessment on Healthy Volunteers

1) Experimental Setup: To investigate the performance of our proposed smart mattress in monitoring RR, five healthy volunteers (two men and three women) were enrolled. Recruited subjects met the following characteristics: age ranging from 24 to 33 years old, body mass between 52 and 96 kg, and height in the range of 160–187 cm. The mattress was placed on a rigid support, and each volunteer was asked to lay his/her torso on it. Before getting started, each subject wore a chest-level wearable system (BioHarness 3.0, Zephyr Technology) used to collect reference respiratory signals at a sampling frequency of 25 Hz during the trial. The smart mattress was connected by means of two fiber-optic patch cables single mode (LC/PC to MU/PC) to the optical interrogator (si255, Hyperion Platform, Micro Optics Inc., Atlanta, GA, USA) and FBGs' output was recorded at a sampling rate of 1 kHz. The experimental protocol consisted of 28 min of consecutive acquisition time, during which the subject changed

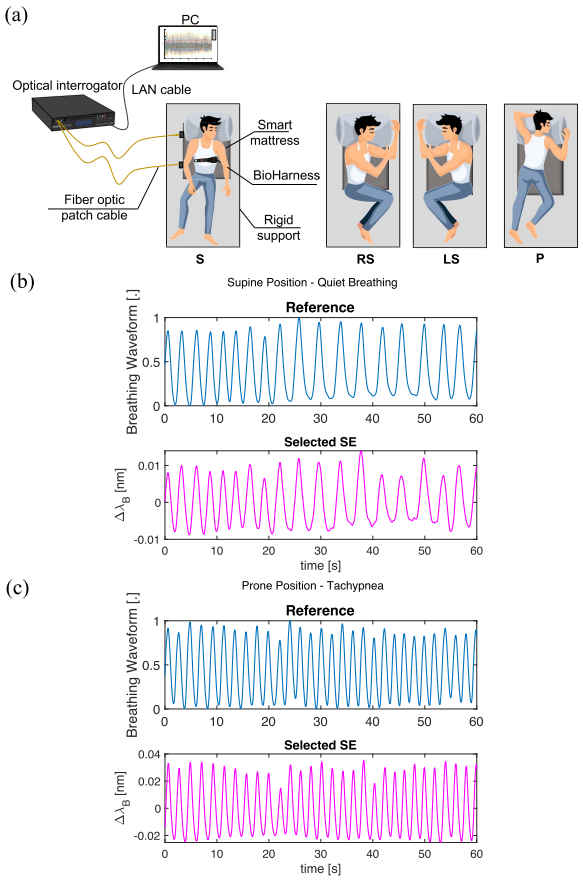

Fig. 6. (a) Experimental setup employed during the experiments. (b) Filtered trends of reference and selected SE during QB in S position during 60 s of acquisition. (c) Filtered trends of reference and selected SE during T in P position during 60 s of acquisition.

four positions (i.e., S, RS, LS, and P) every 7 min [Fig. 6(a)]. For each position, the volunteer was instructed to perform 30 s of apnea, 4.5 min of QB, 30 s of apnea, and 1.5 min of T, timed using a stopwatch. Furthermore, the optical interrogator was connected to a PC via LAN cable for both displaying the $\Delta\lambda_B$ of each sensor during the entire acquisition in real-time through a dedicated developed algorithm in MATLAB and saving data.

2) Data Analysis and Results: Data processing was carried out in MATLAB. Data collected from the reference device and FBGs were synchronized in the first phase, considering the minimum peak of the first apnea performed by each subject at the beginning of the test. Both reference and FBG signals were filtered with a first Butterworth bandpass filter with low and high cut-off frequencies of 0.01 and 1 Hz, respectively, to emphasize breathing-related contributions [46]. Subsequently, data were unpacked and sorted according to the taken up position (i.e., S, RS, LS, and P) and the simulated breathing conditions (i.e., QB and T) to assess the smart mattress under the different proposed conditions. Moreover, $\Delta\lambda_B$ collected by each FBG were undersampled at the same frequency as the reference device (25 Hz). To estimate RR per each subject, position, and condition, it is possible to adopt two different analyses. The first one involves processing the smart mattress collected data in terms of estimated F from the S_F values of each SE, and the second one consists of directly processing $\Delta\lambda_B$ data. Supplementary Materials report the details of the first method and the related results. Here, we present and discuss the results obtained for the second analysis carried out since it allows for better performance. For this purpose, the following steps were performed.

1) All the spectra of the 13 $\Delta\lambda_B$ were computed by using Welch's overlapped segment averaging estimator. Only the $\Delta\lambda_B$ with the highest power was chosen for the next steps.
   As an example, Fig. 6(b) and (c) shows the filtered trends of the reference instrument and the selected SE during 60 s of QB in the S position and T in the P position, respectively, collected from two of the volunteers enrolled in our study. Supplementary Materials report other time graphs collected during one of the experiments.
2) Both the selected SE and the reference data were processed by splitting the signals in sliding windows of 30 s length moving every 1 s. In each window, power spectral density (PSD) plots were estimated by means of Welch's method.
3) Per both the PSDs, the maximum frequency peak ($f_{\max}$) was identified, thus obtaining the RR values of both reference ($\mathrm{RR}^{\mathrm{ref}}$) and selected SE of the mattress ($\mathrm{RR}^{\mathrm{Mattress}}$) for each window via the following equation:
$$\mathrm{RR} = \frac{60}{1/f_{\max}}. \tag{5}$$
   This analysis provided 240 values of $\mathrm{RR}^{\mathrm{ref}}$ and $\mathrm{RR}^{\mathrm{Mattress}}$ each in the case of QB (4.5 min of acquisition time) and 60 values in case of T (1.5 min of recording time).

To quantitatively evaluate the performance of our smart mattress compared to the reference instrument, the mean absolute error (i.e., MAE) was evaluated for all the positions (S, RS, LS, and P) and the simulated conditions (QB and T), as expressed in the following relationship:

$$\mathrm{MAE} = \frac{1}{N}\sum_{k=1}^{N}\left|\mathrm{RR}_k^{\mathrm{Mattress}} - \mathrm{RR}_k^{\mathrm{ref}}\right| \tag{6}$$

where N represents the number of the considered windows, and $\mathrm{RR}_k^{\mathrm{Mattress}}$ and $\mathrm{RR}_k^{\mathrm{ref}}$ the respiratory frequency values estimated by the smart mattress and the reference instrument in the kth window, respectively. Fig. 7 reports the MAE related to QB and T found for all the subjects enrolled and each position (i.e., S, RS, LS, and P). Results reveal MAE is always lower than 0.24 breaths/min in QB and 0.65 breaths/min in T. As evidenced by Fig. 7, the obtained MAE values are comparable under conditions of QB and T for the four positions. Marked differences are evident only for subjects 4 and 5 in LS and P across the two simulated breathing conditions (QB vs. T).

As an additional metric for performance assessment, the mean percentage absolute error (i.e., MAPE) for each condition, position, and subject enrolled was also calculated as follows:

$$\mathrm{MAPE}\ [\%] = \frac{1}{N}\sum_{k=1}^{N}\frac{\left|\mathrm{RR}_k^{\mathrm{Mattress}} - \mathrm{RR}_k^{\mathrm{ref}}\right|}{\mathrm{RR}_k^{\mathrm{ref}}}\cdot 100. \tag{7}$$

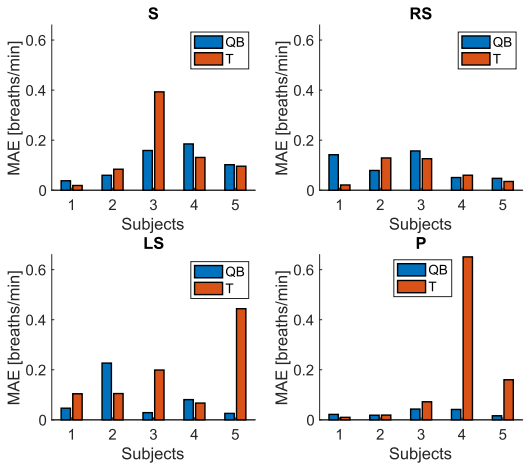

Fig. 7. MAE related to QB and T for each subject enrolled at each position (i.e., S, RS, LS, and P).

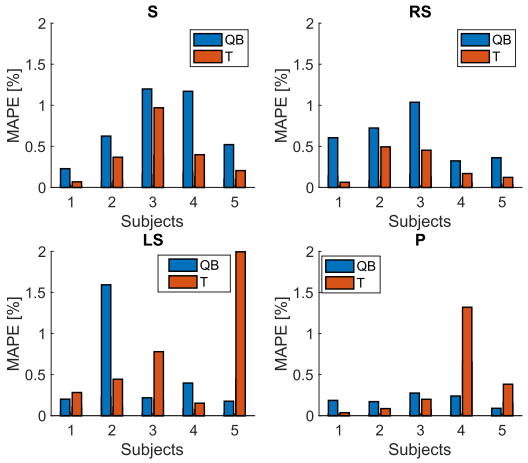

Fig. 8. MAPE related to QB and T for each subject enrolled at each position (i.e., S, RS, LS, and P).

Fig. 8 reports the MAPE values for QB and T conditions, in each position (i.e., S, RS, LS, and P) for all the five subjects enrolled. Results show a maximum MAPE of 1.6% in QB and 2.0% in T.

Finally, a Bland–Altman analysis was carried out to assess the agreement between our system and the reference one, considering RR values estimated in both conditions (QB and T) and for each position (S, RS, LS, and P) (see Fig. 9). The mean of differences (MOD) and limits of agreements (LOAs) allowed us to quantify the bias between $RR^{Mattress}$ and RR^{ref}. Table II reports the MOD $\pm$ LOAs obtained considering both QB and T for all the postures taken up by the volunteers. All the MOD values close to zero prove the strong performance of the proposed solution. Moreover, LOA values are comparable in all the positions (always lower than $\pm$0.99 breaths/min) with slightly higher values in LS.

TABLE II
BLAND–ALTMAN: MOD $\pm$ LOAS OBTAINED CONSIDERING BOTH QB AND T

Position	MOD $\pm$ LOAs [breaths/min]
S	0.01$\pm$0.74
RS	-0.02$\pm$0.78
LS	0.01$\pm$0.99
P	-0.02$\pm$0.69

IV. DISCUSSIONS

In this study, we presented a novel smart mattress based on 13 SEs embedding one FBG each for RR monitoring over time. The proposed solution has numerous points of novelty in terms of design, manufacturing, and characterization. First of all, the use of distributed soft SEs made of silicone rubber has been successfully exploited for the development of a sensing mattress. Unlike other proposed solutions in the literature in which the fiber was only attached to a bottom material [29], [30], [31], [32], [40], [43], our design allowed the complete integration of optical fiber inside multiple silicone layers, thus conferring compactness, high robustness, and resistance to unwanted breakage without compromising the sensitivity to the strain-induced breathing movements, even in the presence of heavy body mass. Moreover, the fiber embedding between two silicone layers with different stiffnesses (i.e., DragonSkin30 for the bottom layer and DragonSkin10 for the top layer) prevented potential strain damping through the material. Second, the mattress dimensions were chosen taking into account literature-available body anthropometric proportions to tackle inter-subject anatomical variability (as detailed in Section III-A) which is pretty uncommon in other solutions and to potentially extend the use of our mattress on a very wide population with different statures taking on the most common sleeping postures. The use of multiple sensors and their serpentine arrangement allow SE distribution over a large surface in contact with the upper and middle portions of the trunk, ensuring at least one sensor can detect RR, regardless of the position taken. This is very important in long-term applications (e.g., during sleeping) since it is plausible that the subject switches his/her position in the bed (such as those simulated in this work). In the literature, some studies proposed the instrumentation of too wide surfaces as the entire bed [29], or too narrow with a single FBG on a plexiglass board as in [30] and [31]. Our approach overcomes these limitations as it offers the instrumentation of the areas most exposed to deformations caused by breathing. Compact systems with reasonable dimensions were, instead, encountered in [38], [43], and [45], although the choice of proposed size was not supported by the authors. Third, before developing the smart mattress, both static and dynamic metrological characterizations were pursued to assess the S_F and $\overline{\text{Hyst}_{\text{err}}\%}$ of each SE, neglected aspects in available studies dealing with fiber optic sensing mats. The linear response of all the SEs suggests a satisfactory adhesion between the fiber and the silicone material; moreover, S_F values were comparable among the manufactured SEs, with a mean value of 14 pm $\cdot$ N^{-1} and a standard deviation equal to just 2 pm $\cdot$ N^{-1}. The differences in S_F values found across the SEs can be attributed to a lack of reproducibility in the fabrication process (e.g., the insufficient pulling force of the optical fiber or small deviations in the FBG positioning within the silicone rubber) and the possible dissimilar interface bonding

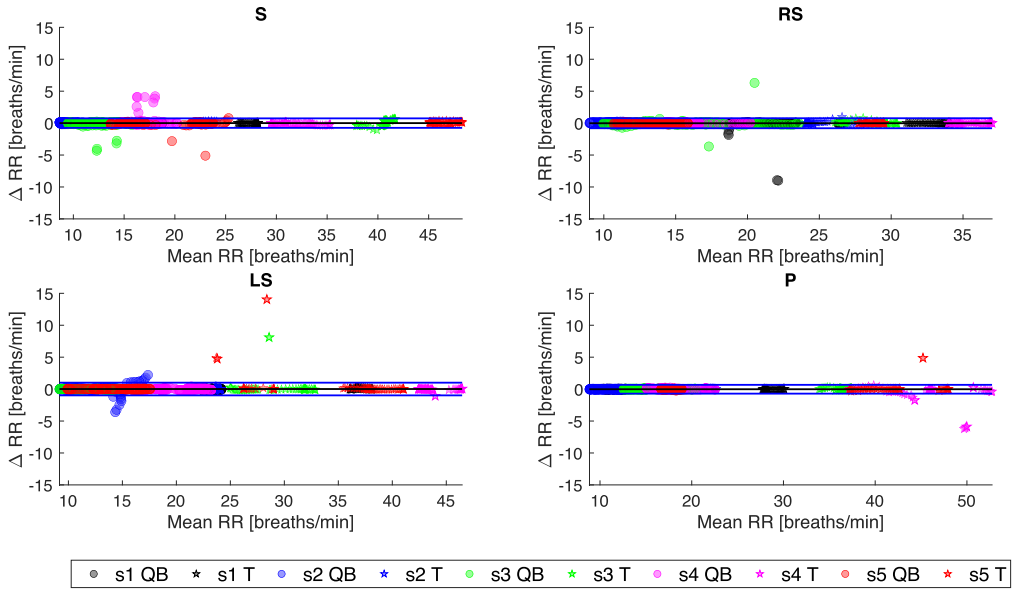

Fig. 9. Bland–Altman analysis plots for each position (S, RS, LS, and P). In the y-axis, the ΔRR [breaths/min] (calculated as $\mathrm{RR}_k^{\mathrm{Mattress}} - \mathrm{RR}_k^{\mathrm{ref}}$) and in the x-axis, the mean RR. In each subplot, MOD is reported with a black continuous line, while LOAs with blue continuous lines.

between the optical fiber and the silicone material. This value is slightly lower than the one of an FBG-based force sensor embedded in a soft rubber (i.e., DragonSkin30) presented in [56] and metrological assessed over a broader range of F (i.e., 0–40 N). The dynamic tests mimicked the scenario of interest by simulating different breathing conditions (i.e., 12, 24, 36, and 60 breaths/min). $\overline{\mathrm{Hyst}_{\mathrm{err}}\%}$ values were always lower than 18%. This result is comparable to or even lower than others obtained in FBG-based wearable systems [57], [58], attesting to the reliability of the proposed system in monitoring breathing phases. Comparing our results with those of fiber optic-based mattresses, only two studies accomplished the metrological process: in one instance only in terms of static response [29], whereas, in the second, repetitive loading cycles are exclusively used to verify the zero-pressure level changes [39]. In [29], although FBGs were employed, the authors did not report the S_F values obtained but only the calibration curve which resulted in linear. This behavior agrees with all the calibration curves we obtained with our SEs. The proposed smart mattress was initially assessed on five healthy volunteers of both sexes in the most common sleeping postures (S, RS, LS, and P) and during different breathing conditions (QB and T) for a total acquisition time of 28 min/subject. Raw data were automatically processed in the frequency domain to first select the most informative SE and then to estimate RR values from its signal with an update time of 1 s. We want to point out that the RR time series were not cleaned for removing outliers. Our system showed an MAE always lower than 0.24 breaths/min in QB and 0.65 breaths/min in T for all positions with a very wide range of measured RR between 8 and 53 breaths/min (see Fig. 8), outperforming other similar studies carried out during QB as [38] (0.24 vs. 0.38 breaths/min) and [22] (0.24 vs. 0.59 breaths/min). The higher MAPE was 2.0% which is less than half of the values reported in other studies dealing with fiber-optic mattresses [30], [31], [32], [45] and half of the one reported for a commercial mattress based on piezoresistive sensors [21]. Bland–Altman analysis revealed MOD close to zero in all the conditions and LOA values comparable in all the sleeping positions, lower than 1.4 breaths/min achieved by [43], 1.5 breaths/min reported in [40], and 4.5 breaths/min in [38]. Instead, comparable LOAs were obtained in [30] and [31] with RR estimated in the time domain and a narrow range of RR (6–32 breaths/min) in the S position than ours. Compared to mattresses instrumented with other sensing technologies, our results outweigh those reported in [22], [34], and [35]. Ranta et al. [22] reported LOAs equal to 2.36 breaths/min for an RR range between 10 and 22 breaths/min, more than two times higher than the worst we obtained (i.e., 0.99 breaths/min for LS). For a piezoresistive mattress, in [34], we found MOD $\pm$ LOAs equal to -5.6 ± 21.5 breaths/min in the case of S position, far from those we obtained in this study on a comparable number of subjects and simulated RR. Worse results in terms of LOAs were also found in [35] for a pressure mattress with LOA values up to 2.08 breaths/min among the same simulated positions (S, RS, LS, and P) in a narrow RR range. Table SII, in Supplementary Materials, also provides further details on the proposed comparisons and other available bed sensors, including some commercially available, used for RR monitoring. Moreover, ΔRR values through the whole range of RR measurements suggest the absence of proportional bias in any condition, although such a finding requires a larger sample size to be confirmed. This emphasizes the advantages offered by the multipoint measurement of breathing-induced force and the adequacy of the user- and position-independent automatic selection of the most informative SE. Furthermore, similar results were obtained on both male and female volunteers.

V. Conclusion

In conclusion, this article reports our research regarding the design, fabrication, metrological characterization, and in-lab assessment of an FBG-based mattress conceived for RR measurement. The complete integration of the 13 SEs (each encasing an FBG) within several layers of silicone material overcame the optical fiber's inherent fragility and afforded comfort to the user. Moreover, the adoption of FBG technology allowed for deploying a multisensor approach, thus monitoring subjects with different anthropometric characteristics and taking different sleeping postures. The promising findings support the suitability of the proposed system to detect RR in a wide range of applications and scenarios. Nevertheless, our study presented some limitations. The first lies in the high cost and bulky dimensions of the interrogation system necessary to enlighten the fiber and pick up the signal from FBGs. Other limitations concern the small number of recruited subjects and the in-lab validation. Therefore, future studies plan to increase the sample size to strengthen the performance analysis of the proposed solution in detecting RR and other respiratory variables. Additionally, we envisage testing smart mattress performance in real-world scenarios (i.e., home settings or hospital wards) and in-long term applications (i.e., during sleeping). In our future analyses, we intend to include benchmarking the proposed system against a reference instrument used in clinical settings (e.g., polysomnograph) and implement algorithms to detect breathing-unrelated movements and mitigate their effects on RR estimation over time.

References

[1] G. Matar, J.-M. Lina, J. Carrier, and G. Kaddoum, "Unobtrusive sleep monitoring using cardiac, breathing and movements activities: An exhaustive review," *IEEE Access*, vol. 6, pp. 45129–45152, 2018.

[2] N. S. Kamel and J. K. Gammack, "Insomnia in the elderly: Cause, approach, and treatment," *Amer. J. Med.*, vol. 119, no. 6, pp. 463–469, Jun. 2006.

[3] D. N. Fairbanks, S. A. Mickelson, and B. T. Woodson, *Snoring and Obstructive Sleep Apnea*. Philadelphia, PA, USA: Lippincott Williams & Wilkins, 2003.

[4] A. S. Baran and A. C. Richert, "Obstructive sleep apnea and depression," *CNS Spectrums*, vol. 8, no. 2, pp. 128–134, 2003.

[5] V. Mohsenin, "Sleep-related breathing disorders and risk of stroke," *Stroke*, vol. 32, no. 6, pp. 1271–1278, Jun. 2001.

[6] F. Roux, C. D'Ambrosio, and V. Mohsenin, "Sleep-related breathing disorders and cardiovascular disease," *Amer. J. Med.*, vol. 108, no. 5, pp. 396–402, 2000.

[7] P. J. Strollo Jr., and R. M. Rogers, "Obstructive sleep apnea," *New England J. Med.*, vol. 334, no. 2, pp. 99–104, 1996.

[8] A. Nicolò, C. Massaroni, E. Schena, and M. Sacchetti, "The importance of respiratory rate monitoring: From healthcare to sport and exercise," *Sensors*, vol. 20, no. 21, p. 6396, Nov. 2020.

[9] M. A. Cretikos, R. Bellomo, K. Hillman, J. Chen, S. Finfer, and A. Flabouris, "Respiratory rate: The neglected vital sign," *Med. J. Austral.*, vol. 188, no. 11, pp. 657–659, 2008.

[10] J. V. Rundo and R. Downey, "Polysomnography," in *Handbook of Clinical Neurology*, vol. 160, pp. 381–392, 2019.

[11] K. E. Bloch, "Polysomnography: A systematic review," *Technol. Health Care*, vol. 5, no. 4, pp. 285–305, 1997.

[12] B. Oeverland, H. Akre, K. J. Kvaerner, and O. Skatvedt, "Patient discomfort in polysomnography with esophageal pressure measurements," *Eur. Arch. Oto-Rhino-Laryngol.*, vol. 262, no. 3, pp. 241–245, Mar. 2005.

[13] C. Massaroni, A. Nicoló, E. Schena, and M. Sacchetti, "Remote respiratory monitoring in the time of COVID-19," *Frontiers Physiol.*, vol. 11, p. 635, May 2020.

[14] C. Brüser, C. H. Antink, T. Wartzek, M. Walter, and S. Leonhardt, "Ambient and unobtrusive cardiorespiratory monitoring techniques," *IEEE Rev. Biomed. Eng.*, vol. 8, pp. 30–43, 2015.

[15] Y.-L. Wang et al., "Low-cost wearable sensor based on a D-shaped plastic optical fiber for respiration monitoring," *IEEE Trans. Instrum. Meas.*, vol. 70, pp. 1–8, 2021.

[16] S. Nizami, A. Bekele, M. Hozayen, K. J. Greenwood, J. Harrold, and J. R. Green, "Measuring uncertainty during respiratory rate estimation using pressure-sensitive mats," *IEEE Trans. Instrum. Meas.*, vol. 67, no. 7, pp. 1535–1542, Jul. 2018.

[17] G. Karacocuk et al., "Inertial sensor-based respiration analysis," *IEEE Trans. Instrum. Meas.*, vol. 68, no. 11, pp. 4268–4275, Nov. 2019.

[18] Q. Zhai, X. Han, Y. Han, J. Yi, S. Wang, and T. Liu, "A contactless on-bed radar system for human respiration monitoring," *IEEE Trans. Instrum. Meas.*, vol. 71, pp. 1–10, 2022.

[19] M. Cohen-McFarlane, S. Bennett, B. Wallace, R. Goubran, and F. Knoefel, "Bed-based health monitoring using pressure sensitive technology: A review," *IEEE Instrum. Meas. Mag.*, vol. 24, no. 2, pp. 13–23, Apr. 2021.

[20] G. G. Mora, J. M. Kortelainen, E. R. P. Hernández, M. Tenhunen, A. M. Bianchi, and M. O. Méndez, "Evaluation of pressure bed sensor for automatic SAHS screening," *IEEE Trans. Instrum. Meas.*, vol. 64, no. 7, pp. 1935–1943, Jul. 2015.

[21] J. Ben-Ari, E. Zimlichman, N. Adi, and P. Sorkine, "Contactless respiratory and heart rate monitoring: Validation of an innovative tool," *J. Med. Eng. Technol.*, vol. 34, nos. 7–8, pp. 393–398, Oct. 2010.

[22] J. Ranta, T. Aittokoski, M. Tenhunen, and M. Alasaukko-Oja, "EMFIT QS heart rate and respiration rate validation," *Biomed. Phys. Eng. Exp.*, vol. 5, no. 2, 2019, Art. no. 025016.

[23] M. J. Breteler et al., "Vital signs monitoring with wearable sensors in high-risk surgical patients: A clinical validation study," *Anesthesiology*, vol. 132, no. 3, pp. 424–439, 2020.

[24] A. Bekele et al., "Real-time neonatal respiratory rate estimation using a pressure-sensitive mat," in *Proc. IEEE Int. Symp. Med. Meas. Appl. (MeMeA)*, Jun. 2018, pp. 1–5.

[25] P. Chow, G. Nagendra, J. Abisheganaden, and Y. Wang, "Respiratory monitoring using an air-mattress system," *Physiolog. Meas.*, vol. 21, no. 3, p. 345, 2000.

[26] Y. Chee, J. Han, J. Youn, and K. Park, "Air mattress sensor system with balancing tube for unconstrained measurement of respiration and heart beat movements," *Physiolog. Meas.*, vol. 26, no. 4, p. 413, 2005.

[27] M. Brink, C. H. Müller, and C. Schierz, "Contact-free measurement of heart rate, respiration rate, and body movements during sleep," *Behav. Res. Methods*, vol. 38, no. 3, pp. 511–521, Aug. 2006.

[28] J. H. Shin, Y. J. Chee, D. U. Jeong, and K. S. Park, "Nonconstrained sleep monitoring system and algorithms using air-mattress with balancing tube method," *IEEE Trans. Inf. Technol. Biomed.*, vol. 14, no. 1, pp. 147–156, Jan. 2010.

[29] J. Hao, M. Jayachandran, P. L. Kng, S. F. Foo, P. W. A. Aung, and Z. Cai, "FBG-based smart bed system for healthcare applications," *Frontiers Optoelectron. China*, vol. 3, no. 1, pp. 78–83, Mar. 2010.

[30] Ł. Dziuda, M. Krej, and F. W. Skibniewski, "Fiber Bragg grating strain sensor incorporated to monitor patient vital signs during MRI," *IEEE Sensors J.*, vol. 13, no. 12, pp. 4986–4991, Dec. 2013.

[31] Ł. Dziuda, F. W. Skibniewski, M. Krej, and P. M. Baran, "Fiber Bragg grating-based sensor for monitoring respiration and heart activity during magnetic resonance imaging examinations," *J. Biomed. Opt.*, vol. 18, no. 5, May 2013, Art. no. 057006.

[32] Z. Chen, D. Lau, J. T. Teo, S. H. Ng, X. Yang, and P. L. Kei, "Simultaneous measurement of breathing rate and heart rate using a microbend multimode fiber optic sensor," *J. Biomed. Opt.*, vol. 19, no. 5, May 2014, Art. no. 057001.

[33] R.-Y. Yang, A. Bendjoudi, N. Buard, and P. Boutouyrie, "Pneumatic sensor for cardiorespiratory monitoring during sleep," *Biomed. Phys. Eng. Exp.*, vol. 5, no. 5, Aug. 2019, Art. no. 055014.

[34] N. Carbonaro, M. Laurino, L. Arcarisi, D. Menicucci, A. Gemignani, and A. Tognetti, "Textile-based pressure sensing matrix for in-bed monitoring of subject sleeping posture and breathing activity," *Appl. Sci.*, vol. 11, no. 6, p. 2552, Mar. 2021.

[35] G. Matar, G. Kaddoum, J. Carrier, and J.-M. Lina, "Kalman filtering for posture-adaptive in-bed breathing rate monitoring using bed-sheet pressure sensors," *IEEE Sensors J.*, vol. 21, no. 13, pp. 14339–14351, Jul. 2021.

[36] S. Isono et al., "Contact-free unconstraint respiratory measurements with load cells under the bed in awake healthy volunteers: Breath-by-breath comparison with pneumotachography," *J. Appl. Physiol.*, vol. 126, no. 5, pp. 1432–1441, 2019.

[37] W. Y. Chang, C. C. Huang, C. C. Chen, C. C. Chang, and C. L. Yang, "An enhanced sensing application based on a flexible projected capacitive-sensing mattress," *Sensors*, vol. 14, no. 4, pp. 6922–6937, 2014.

[38] I. Sadek, E. Seet, J. Biswas, B. Abdulrazak, and M. Mokhtari, "Non-intrusive vital signs monitoring for sleep apnea patients: A preliminary study," *IEEE Access*, vol. 6, pp. 2506–2514, 2018.

[39] D. Sartiano and S. Sales, "Low cost plastic optical fiber pressure sensor embedded in mattress for vital signal monitoring," *Sensors*, vol. 17, no. 12, p. 2900, Dec. 2017.

[40] G. He et al., "Heart rate and respiration rate detection by optical fiber mattress using statistical classification spectrum analysis," *Biomed. Phys. Eng. Exp.*, Feb. 2019. [Online]. Available: https://iopscience.iop.org/article/10.1088/2057-1976/ab072f/pdf

[41] S. Peng, K. Xu, S. Bao, Y. Yuan, C. Dai, and W. Chen, "Flexible electrodes-based smart mattress for monitoring physiological signals of heart and autonomic nerves in a non-contact way," *IEEE Sensors J.*, vol. 21, no. 1, pp. 6–15, Jan. 2021.

[42] M. Laurino, L. Arcarisi, N. Carbonaro, A. Gemignani, D. Menicucci, and A. Tognetti, "A smart bed for non-obtrusive sleep analysis in real world context," *IEEE Access*, vol. 8, pp. 45664–45673, 2020.

[43] S. Wang et al., "Noninvasive monitoring of vital signs based on highly sensitive fiber optic mattress," *IEEE Sensors J.*, vol. 20, no. 11, pp. 6182–6190, Jun. 2020.

[44] Z. Wang et al., "A piezoresistive array based force sensing technique for sleeping posture and respiratory rate detection for SAS patients," *IEEE Sensors J.*, early access, Dec. 13, 2021, doi: 10.1109/JSEN.2021.3134823.

[45] P. Han et al., "Low-cost plastic optical fiber sensor embedded in mattress for sleep performance monitoring," *Opt. Fiber Technol.*, vol. 64, Jul. 2021, Art. no. 102541.

[46] F. de Tommasi, D. L. Presti, M. Carassiti, E. Schena, and C. Massaroni, "Smart mattress based on fiber Bragg grating sensors for respiratory monitoring: A feasibility test," in *Proc. IEEE Int. Workshop Metrology Ind. 4.0 IoT*, Jun. 2021, pp. 532–537.

[47] C. Massaroni, M. Zaltieri, D. L. Presti, A. Nicolò, D. Tosi, and E. Schena, "Fiber Bragg grating sensors for cardiorespiratory monitoring: A review," *IEEE Sensors J.*, vol. 21, no. 13, pp. 14069–14080, Jul. 2021.

[48] D. L. Presti et al., "Fiber Bragg gratings for medical applications and future challenges: A review," *IEEE Access*, vol. 8, pp. 156863–156888, 2020.

[49] K. O. Hill and G. Meltz, "Fiber Bragg grating technology fundamentals and overview," *J. Lightw. Technol.*, vol. 15, no. 8, pp. 1263–1276, Aug. 1997.

[50] T. Erdogan, "Fiber grating spectra," *J. Lightw. Technol.*, vol. 15, no. 8, pp. 1277–1294, Aug. 1997.

[51] A. Othonos, K. Kalli, D. Pureur, and A. Mugnier, "Fibre Bragg gratings," in *Wavelength Filters in Fibre Optics*. Cham, Switzerland: Springer, 2006, pp. 189–269.

[52] C. Chourpiliadis and A. Bhardwaj, *Physiology, Respiratory Rate*. Treasure Island, FL, USA: StatPearls, 2022.

[53] C. Russo, F. Mocera, and A. Somà, "MEMS sensors for sport engineer applications," *IOP Conf. Ser., Mater. Sci. Eng.*, vol. 1038, no. 1, Feb. 2021, Art. no. 012056.

[54] C. Massaroni, G. Senesi, E. Schena, and S. Silvestri, "Analysis of breathing via optoelectronic systems: Comparison of four methods for computing breathing volumes and thoraco-abdominal motion pattern," *Comput. Methods Biomech. Biomed. Eng.*, vol. 20, no. 16, pp. 1678–1689, 2017.

[55] Smooth-On. *Dragon Skin™ Series, High Performance Silicone Rubber*. Accessed: Mar. 8, 2022. [Online]. Available: https://www.smoothon.com/product-line/dragon-skin/

[56] F. De Tommasi, D. Lo Presti, F. Virgili, C. Massaroni, E. Schena, and M. Carassiti, "Soft system based on fiber Bragg grating sensor for loss of resistance detection during epidural procedures: In silico and in vivo assessment," *Sensors*, vol. 21, no. 16, p. 5329, Aug. 2021.

[57] J. Di Tocco et al., "A wearable system based on flexible sensors for unobtrusive respiratory monitoring in occupational settings," *IEEE Sensors J.*, vol. 21, no. 13, pp. 14369–14378, Jul. 2021.

[58] D. L. Presti et al., "Wearable system based on flexible FBG for respiratory and cardiac monitoring," *IEEE Sensors J.*, vol. 19, no. 17, pp. 7391–7398, May 2019.

Francesca De Tommasi (Student Member, IEEE) received the M.Sc. degree (cum laude) in biomedical engineering from Università Campus Bio-Medico di Roma, Rome, Italy, in 2020, where she is currently pursuing the Ph.D. degree in bioengineering.

Her research interests focus on the development of fiber Bragg grating-based measurement systems for biomedical applications.

Daniela Lo Presti (Member, IEEE) received the Ph.D. degree in bioengineering from Università Campus Bio-Medico di Roma, Rome, Italy, in 2020.

She is currently an Assistant Professor at Università Campus Bio-Medico di Roma. Her research interests focus on the design, fabrication, and assessment of fiber Bragg grating sensor-based tools and wearables for medical and biomedical applications.

Michele Arturo Caponero received the bachelor's degree in physics from the University of Bari, Bari, Italy, in 1986.

He is a Researcher with the Photonics Micro- and Nanostructures Laboratory, Research Center of Frascati, ENEA, Frascati, Rome, Italy. His research interests include distributed fiber-optic-based sensors for structural monitoring and interferometric technique development.

Massimiliano Carassiti is currently an Anesthesiologist and an Associate Professor of anesthesia at Università Campus Bio-Medico di Roma, Rome, Italy. His main research interests include anesthesiology, intensive care medicine, pain medicine and management, and the development of smart systems to support physicians during epidural procedures.

Emiliano Schena (Senior Member, IEEE) received the Ph.D. degree from Università Campus Bio-Medico di Roma, Rome, Italy, in 2007.

He is a Full Professor of measurements with Università Campus Bio-Medico di Roma. His main research interests include the design and assessment of wearable systems for vital signs monitoring, applications of fiber-optic sensors in medicine, and thermal ablation for cancer removal.

Carlo Massaroni (Senior Member, IEEE) received the Ph.D. degree in biomedical engineering from Università Campus Bio-Medico di Roma, Rome, Italy, in 2017.

He is currently an Assistant Professor of measurements with Università Campus Bio-Medico di Roma. His research interests include the design, development, and testing of wearable devices and unobtrusive measuring systems for medical applications.

Open Access funding provided by 'Università "Campus Bio-Medico" di Roma' within the CRUI CARE Agreement